



Article

Identifying and Characterizing Dust-Induced Cirrus Clouds by Synergic Use of Satellite Data

Samaneh Moradikian ^{1,2}, Sanaz Moghim ^{1,†}  and Gholam Ali Hoshyaripour ^{2,*,†} 

¹ Department of Civil Engineering, Sharif University of Technology, Tehran P.O. Box 11155-9161, Iran; smkian12@gmail.com (S.M.); moghim@sharif.edu (S.M.)

² Institute of Meteorology and Climate Research Troposphere Research, Karlsruhe Institute of Technology, 76131 Karlsruhe, Germany

* Correspondence: gholamali.hoshyaripour@kit.edu

† These authors contributed equally to this work.

Highlights

What are the main findings?

- An algorithm was developed to identify dust-induced cirrus clouds using long-term observational data from the CALIPSO satellite. This method provides a systematic way to identify occurrences of these clouds.
- Dust-induced cirrus clouds are thicker, form at higher altitudes, and are more frequent in the studied regions of the Aral Sea and the Iberian Peninsula. Their prevalence in the Aral Sea peaks in spring, correlating with high dust concentrations.

What is the implication of the main finding?

- The research provides methodological advancements for detecting dust-induced cirrus clouds and offers a statistical basis for understanding how mineral dust influences their formation and frequency.
- The findings enhance our understanding of the interaction between mineral dust and cloud microphysics, which has important implications for improving global climate modeling and weather forecasting by integrating a dust–cloud feedback mechanism.



Academic Editor: Manuel Antón

Received: 26 April 2025

Revised: 8 September 2025

Accepted: 9 September 2025

Published: 13 September 2025

Citation: Moradikian, S.; Moghim, S.; Hoshyaripour, G.A. Identifying and Characterizing Dust-Induced Cirrus Clouds by Synergic Use of Satellite Data. *Remote Sens.* **2025**, *17*, 3176. <https://doi.org/10.3390/rs17183176>

Copyright: © 2025 by the authors. Licensee MDPI, Basel, Switzerland. This article is an open access article distributed under the terms and conditions of the Creative Commons Attribution (CC BY) license (<https://creativecommons.org/licenses/by/4.0/>).

Abstract

Cirrus clouds cover 25% of the Earth at any given time. However, significant uncertainties remain in our understanding of cirrus cloud formation, in particular, how it is impacted by aerosols. This study investigates the formation and properties of dust-induced cirrus clouds using long-term observational datasets, focusing on Central Asia’s Aral Sea region and the Iberian Peninsula. We identify cirrus events influenced by mineral dust using an algorithm that uses CALIPSO satellite data through spatial and temporal proximity analysis. Results indicate significant seasonal and regional variations in the prevalence of dust-induced cirrus clouds, with spring emerging as the peak season for the Aral Sea and high-altitude Saharan dust transport influencing the Iberian Peninsula. With the help of DARDAR-Nice data, we characterize dust-induced cirrus clouds as being thicker, forming at higher altitudes, and exhibiting distinct microphysical properties, including reduced ice crystal concentrations and smaller frozen water content. Furthermore, a statistical test using a non-parametric Mann–Whitney U test is employed and confirms the robustness of the study. These findings enhance our understanding of the interactions between mineral dust and cloud microphysics, with implications for global climate modeling and weather forecasting. This study provides methodological advancements for dust-induced cloud

detection and highlights the need for integrating a dust–cloud feedback mechanism in weather and climate models.

Keywords: cirrus clouds; CALIPSO; DARDAR-Nice; dust-induced cirrus cloud; aerosol–cloud interaction; heterogeneous ice nucleation

1. Introduction

Cirrus clouds, composed of ice crystals, form in the upper troposphere [1]. Similar to other clouds, they impact the Earth’s radiative budget by reflecting solar radiation while absorbing and emitting terrestrial infrared radiation [2]. At any given time, they cover around 20% to 25% of the Earth’s surface [3]. The formation of these clouds can occur through various mechanisms, primarily driven by the cooling of rising air masses or radiative processes. The ice particle formation occurs through two nucleation mechanisms: homogeneous ice nucleation, involving soluble aerosol particles or water droplets, and heterogeneous ice nucleation, involving insoluble ice-nucleating particles (INPs) [4,5]. Homogeneous freezing of soluble aerosol particles is most common under conditions of strong cooling rates and high supersaturations with respect to ice (relative humidity of approximately 150%) [5–7]. Conversely, the presence of INPs leads to heterogeneous ice nucleation at lower relative humidity levels than homogeneous freezing [8,9]. In essence, crystalline or solid aerosols acting as INPs can dramatically reduce the energy barrier required for ice nucleation, promoting heterogeneous nucleation [10].

Mineral dust is known as the primary type of INP in the upper troposphere [11–14]. In situ studies, such as Cziczo et al. (2013), highlight the prevalence of dust as the most common cirrus INP in multiple cirrus events and estimate that dust was the predominant cirrus INP type globally [15]. In addition, observational studies further emphasize the significant role of dust aerosols in influencing cirrus cloud formation and properties. Dust-induced cirrus clouds are a type of cirrus cloud formed by the induction of dust particles through heterogeneous ice nucleation. The formation of these clouds could be because of a solely heterogeneous ice nucleation regime or a competition between homogeneous and heterogeneous ice nucleation. Froyd et al. (2022) [11] reported that the percentage of dust-induced cirrus clouds in the northern extra-tropics is 75–93% seasonally. Despite this significant prevalence, systematic methods for identifying dust-induced cirrus clouds in observational data remain limited.

Modeling dust-induced cirrus clouds can help understand the underlying processes and interactions, yet poses several challenges that limit the accuracy of predictions. Variability in microphysical properties complicates accurate modeling. Global models often struggle to capture the small-scale variability of aerosols [13,14], and their long time steps are unable to capture cloud formation details [11]. Moreover, the difficulty of direct observation and the lack of comprehensive dust aerosol abundance measurements make simulating high-altitude ice nucleation particularly challenging. Consequently, models frequently fail to accurately represent the complex microphysical processes and aerosol impacts on ice formation, thus leading to significant uncertainties. For example, Weger et al. (2018) reported substantial underestimation in cloud cover and other cloud-related variables when modeling the impact of mineral dust on cirrus cloud formation during a Saharan dust event [16]. An analysis of 49 dust days over Central Europe between January 2018 and March 2022 using dust, weather forecasting, and satellite data. The results showed that missing dust effects on cloud formation lead to significant underestimations of cloudiness and overestimations of surface radiation in the weather forecast [17]. In another study,

simulated five Saharan dust episodes over Europe, including a sub-grid parameterization for dust-induced cirrus clouds. This dusty cirrus parameterization resulted in the formation of dust-induced cirrus clouds and significant improvements in the prediction of cloudiness and radiation [18].

Most modeling studies on dust-induced cirrus clouds have focused on an individual or a limited number of case studies. High-quality, long-term observational data offer the potential to extend case-study-based regional insights to a global scale, providing a more comprehensive understanding of these cloud systems. Active remote sensing instruments, such as lidar and cloud radar, have proven invaluable for the continuous monitoring of cirrus cloud boundaries and properties at high spatial and temporal resolutions [15].

Studies using long-term observational data on dust-induced cirrus clouds unraveled a significant gap in the current understanding of this atmospheric phenomenon [19]. Enhancing our comprehension of the microphysical properties of dust-induced cirrus clouds can assist in decreasing uncertainty in weather forecasting, global climate models, and climate change projections, as well as aid in evaluating climate intervention strategies [18].

In this study, we aim to advance the understanding of dust-induced cirrus clouds by developing a detection method using observational data, analyzing their frequency, and conducting a statistical analysis of their unique properties. We have developed an algorithm for detecting dust-induced cirrus clouds based on observational data and applied it to long-term case studies in Asia and Europe. Using several coexisting datasets, we investigate the different properties of these cloud types. Section 2 provides a brief description of the datasets, methods, proposed algorithm, and detailed case studies. Section 3 includes results and discussions, followed by conclusions in Section 4.

2. Materials and Methods

2.1. Datasets

2.1.1. CALIOP

The Cloud-Aerosol Lidar with Orthogonal Polarization (CALIOP), onboard the CALIPSO satellite launched in April 2006, provided the observational data for this study [20,21].

CALIOP data offer vertical and horizontal profiles of aerosol and cloud distributions in various datasets. The CALIPSO Level 2 lidar vertical feature mask (VFM) data product is invaluable for atmospheric research due to its vertical profiling, global coverage, long-term data record, aerosol–cloud and aerosol typing discrimination capabilities [22]. Additional information about the VFM, including aerosol and cloud subtypes, can be obtained from the atmospheric volume description product. Cloud subtype products can identify “cirrus,” while aerosol subtype products can identify “dust” and “polluted dust.” In this research, both dust and polluted dust aerosol subtypes are treated as a single category of dust within the algorithm and its outcomes.

In addition, CALIPSO Cloud and Aerosol Profile Products incorporate temperature profiles derived from the Modern-Era Retrospective Analysis for Research and Applications, Version 2 (MERRA-2) dataset. MERRA-2, developed by NASA’s Global Modeling and Assimilation Office (GMAO), is a state-of-the-art atmospheric reanalysis that assimilates satellite observations and ground-based measurements to provide comprehensive climate data. Within the CALIPSO products, the MERRA-2 temperature data are used to provide atmospheric temperature to help distinguish between different clouds and aerosols [22].

2.1.2. DARDAR-Nice

Satellite retrievals of the ice crystal number concentration (Nice) profiles derived from lidar and radar observations are provided by DARDAR-Nice and are employed to estimate

the microphysical properties of the cirrus clouds [20,21,23]. This dataset facilitates the recovery of ice cloud parameters from CALIOP observations, offering a vertical resolution of 60 m and ice crystal number concentrations along the CloudSat footprint (1.7 km). DARDAR-Nice includes details regarding the distance of each layer to the top of the cloud and allows for calculations to determine cloud thickness, providing insights into the vertical span of clouds.

2.2. Analysis Method

To analyze the interaction between dust and cirrus clouds, we developed an algorithm that identifies dust-induced events based on the proximity of dust particles to cirrus clouds. Many studies confirmed that if a cirrus cloud is located in a dust layer, the dust–cloud interaction is thought to occur [23–26]. An analysis evaluated two cirrus cloud events, and the idea behind their case selection is that dust particles can be observed close to cirrus clouds in their vertical or horizontal directions, based on the CALIPSO data. Their analysis showed that both of the cases were dust-induced cirrus clouds [24].

Additionally, in another study using ground-based polarization lidar, cirrus clouds associated with transported dust layers were detected 22 times over Wuhan, China, between 2012 and 2018. Cases were selected based on the presence of dust layers affecting cirrus cloud formation, with criteria including special thickness for the dust layers and layers above a special altitude [27]. All cases were identified as dust-induced cirrus clouds, 3 cases as competition between two nucleation regimes, and the rest revealed that only heterogeneous nucleation was involved [25].

The fundamental concept of the algorithm is to find events where there is enough dust in the exact vicinity of cirrus clouds to be considered a dust-induced cirrus event. For the dust and cloud layers to be considered as connected, there must be a spatial overlap between them (exact vicinity), either vertically or horizontally [24,27]. This methodology of using spatial and temporal proximity as a primary indicator for dust–aerosol interaction is a well-established approach in observational studies where direct causal evidence is not available [24,25,27]. The fundamental assumption, supported by these studies, is that the presence of a sufficient quantity of dust in the immediate vicinity of a newly forming cirrus cloud creates the necessary conditions for heterogeneous nucleation. Therefore, this algorithm provides a systematic and operationally convenient framework for identifying large-scale occurrences of cirrus clouds that have a high probability of being ‘dust-induced’.

The VFM makes classification decisions using cloud top pressure/altitude, cloud opacity, and cloud fraction. An important property of the VFM dataset is that a cell can only be one type of cloud or aerosol (e.g., cirrus or dust), which enables the algorithm to consider them connected. To improve the accuracy of identifying cirrus clouds, temperature is incorporated as a constraint in the algorithm. The algorithm assumes a temperature threshold of less than $-33\text{ }^{\circ}\text{C}$ to discriminate cirrus clouds [18]. The procedure of the algorithm includes the following (see flowchart in Figure 1): (1) load events for each day, (2) checking for the presence of cirrus clouds, and if present, (3) checking if the cirrus cloud meets the temperature constraint, and if yes, (4) checking for a sufficient amount of dust particles (above the threshold) in the exact vicinity of the cirrus clouds, either horizontally or vertically. If there are enough dust particles, the event is marked as a dust-induced cirrus cloud event; otherwise, it is considered a normal cirrus cloud event. The final result is a calendar categorizing each day as a (1) no cirrus day, (2) normal cirrus day, or (3) dust-induced cirrus day.

To have a clear definition of the sufficient amount of dust particles, the threshold, which is widely used in various studies [25,27], is the minimum length or width of the dust layer needed to be considered coupled with the cirrus cloud. In the proposed algorithm,

the dust layer must exceed 1 km in length or width. For cirrus formation altitudes (8.2 to 20.2 km) in the VFM data, the horizontal resolution is 1 km. Thus, having at least two adjacent cells (2 km of dust) next to the cirrus clouds is sufficient as a horizontal threshold. Similarly, since the vertical resolution is 60 m, having 17 dust cells in a column next to the cirrus cloud satisfies the vertical threshold. Some cases may meet both vertical and horizontal thresholds.

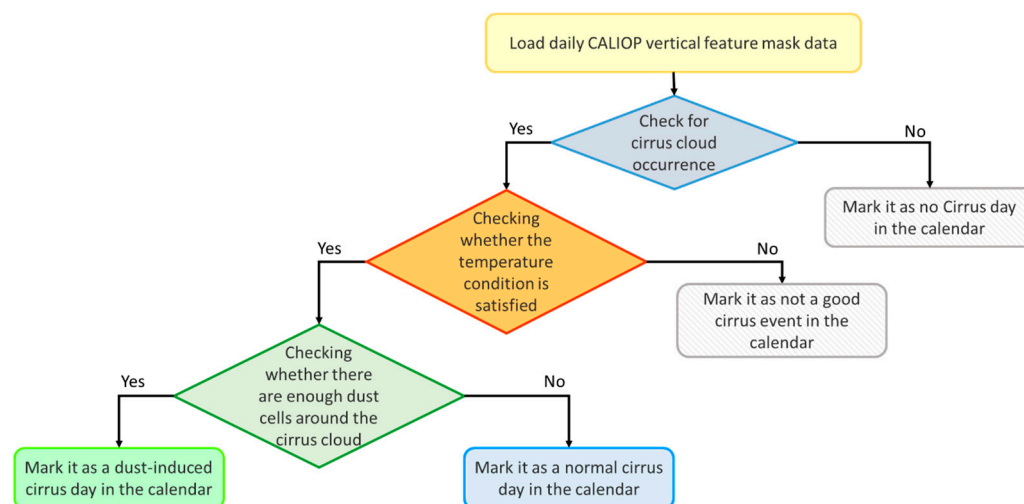


Figure 1. Schematic flowchart of the proposed algorithm.

For evaluating the robustness of the algorithm and being able to quantify the uncertainty of the thresholds, a comprehensive sensitivity analysis has been conducted. As mentioned before, there are two horizontal and vertical thresholds associated with the algorithm. The sensitivity analysis involves systematically varying horizontal and vertical thresholds as follows:

- Horizontal threshold: we tested a “low-restricted” scenario requiring only one adjacent dust cell (1 km) and a “restricted” scenario requiring four adjacent cells (4 km) compared to the original two-cell (2 km) requirement.
- Vertical threshold: we tested a “low-restricted” scenario of 10 adjacent cells (~0.6 km) and a “restricted” scenario of 34 cells (~2 km) compared to the original 17-cell (~1 km) requirement.

The original threshold for the untested dimension was held constant during each analysis.

2.2.1. Analyzing Cloud Properties

After implementing the proposed algorithm and having the dust-induced cirrus calendar, we used a dataset provided by Jeggle et al. (2023) that contains all cirrus cloud events [28]. The dataset comprises detected cirrus clouds by DARDAR-Nice over a large study domain. Throughout the analysis, the dataset is referred to as the ‘Jeggle dataset’. The combination of the two datasets will go through the following two steps: first, finding the shared events between the two datasets (i.e., the same dates of the cirrus cloud occurrence from the VFM and the Jeggle dataset), and second, assigning a label of each cirrus event using the calendar data. As a result, the cirrus cloud events and their corresponding variables are separated into two categories, including normal cirrus events and dust-induced cirrus events. The two categories allow us to investigate the different properties of these two types of cirrus clouds.

To quantitatively assess whether the observed differences in properties between dust-induced and normal cirrus cloud populations were statistically significant, we employed hypothesis testing. Given that many atmospheric variables do not follow a normal (Gaus-

sian) distribution [29], the non-parametric Mann–Whitney U test was chosen. This test is robust for comparing two independent groups without making assumptions about the underlying data distribution [30].

For each variable tested, the null hypothesis was that the data from the two groups (dust-induced and normal) were drawn from the same distribution. A significance level (p -value) of 0.05 was used as the threshold for rejecting the null hypothesis.

2.3. Case Studies

To illustrate our methodology, we use case studies in two regions with significant dust activities: Central Asia (Aral Sea region~490,000 km²) and the Iberian Peninsula (~10⁶ km²). The former serves as a showcase for our analysis algorithm to identify dust-induced cirrus clouds in the long-term dataset of the CALIOP. The latter, in addition to identifying dust-induced cirrus clouds in the CALIOP data, employs the DARDAR-Nice data to analyze and understand the underlying processes and properties. The analysis of these datasets provides a comprehensive understanding of the formation and characteristics of the dust-induced cirrus clouds in these regions.

2.3.1. Central Asia—Aral Sea Region

Central Asia, including the Aral Sea region, is an exceptional area for studying the connection between dust particles and cirrus cloud formation. The Aral Sea is located on the global dust belt [31] and is also reported as one of the active dust sources in Central Asia [32]. Additionally, evaluations using observational data and models show that dust is the predominant aerosol subtype in the Aral Sea region [33], emphasizing the importance of studying the dust and cirrus cloud formation [34]. The study domain for this case study covers the Aral Sea region (Figure 2a,b). The analysis uses the CALIPSO VFM dataset from mid-2006 to 2021 and includes both day and night data.

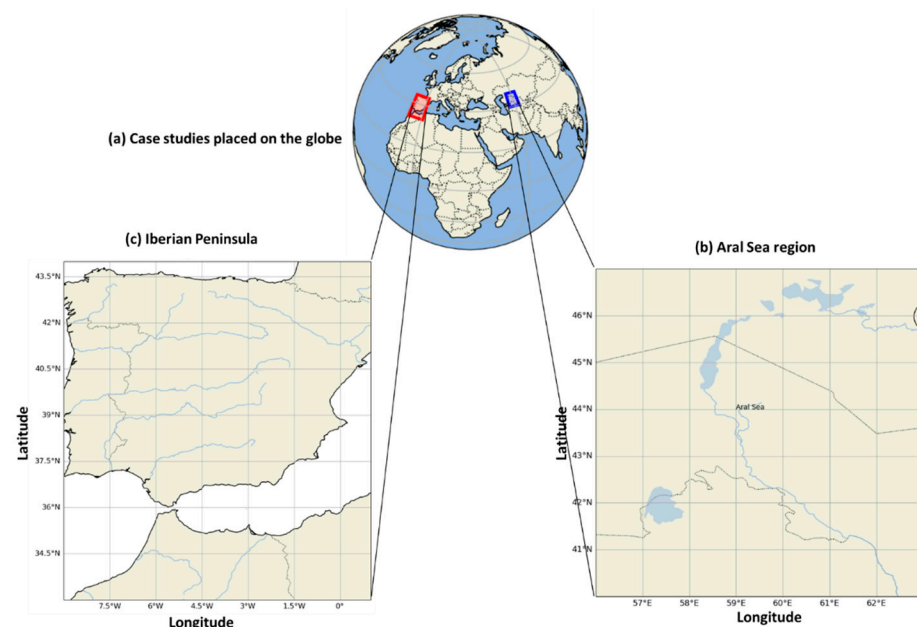


Figure 2. Case studies: (a) location of both case studies, (b) the Aral Sea region, and (c) the Iberian Peninsula.

Process of Cross-Validation

To ensure the robustness of the findings, this study uses cross-validation of the identified dust-induced events by the proposed algorithm with different datasets. The procedure includes the following steps: in the first step, 5% of the dust-induced cirrus cloud events

are randomly selected (90 cases). Then, the desired events over the study region in the Worldview platform are identified based on the specific conditions of the cirrus clouds and dust particles.

- (1) Cloud top temperature (from MODIS): it should be lower than -38° for cirrus clouds [18,35–37].
- (2) Cloud top height (from MODIS): it should be from 8 km [37–39] to 20 km [40,41], which is a normal altitude for cirrus cloud formation.
- (3) Aerosol Optical Depth (AOD from MODIS and VIIRS): it should be more than 0.2 to indicate the presence of dust particles [42–44].

2.3.2. Iberian Peninsula

The Iberian Peninsula (Figure 2a,c) is an ideal location for studying cirrus cloud formation and the impact of Saharan dust transport due to its proximity to the Sahara Desert. This proximity results in frequent and significant dust transport events [45–47]. These events influence cloud formation and atmospheric conditions, providing ample opportunities to observe and analyze changes in aerosol properties, cloud formation processes, and air quality, making this area an excellent natural laboratory for such studies [16,23]. This study uses the nighttime data of the years 2007 to 2009 for analysis in this case study.

3. Results

3.1. Aral Sea

In the 16 years of the data, the total number of available overpasses is 4459, out of which 2726 contain cirrus clouds (approximately 60% of cases). Excluding 18 cases that do not meet the temperature thresholds of -33°C or -38°C , 2708 valid cirrus cloud cases remain. Among them, 1787 were identified as dust-induced cirrus clouds using the algorithm. Detailed annual data are provided in Figure 3. Notably, the CALIPSO dataset for 2006 covers only half the year, resulting in a significantly lower number of cases compared to subsequent years.

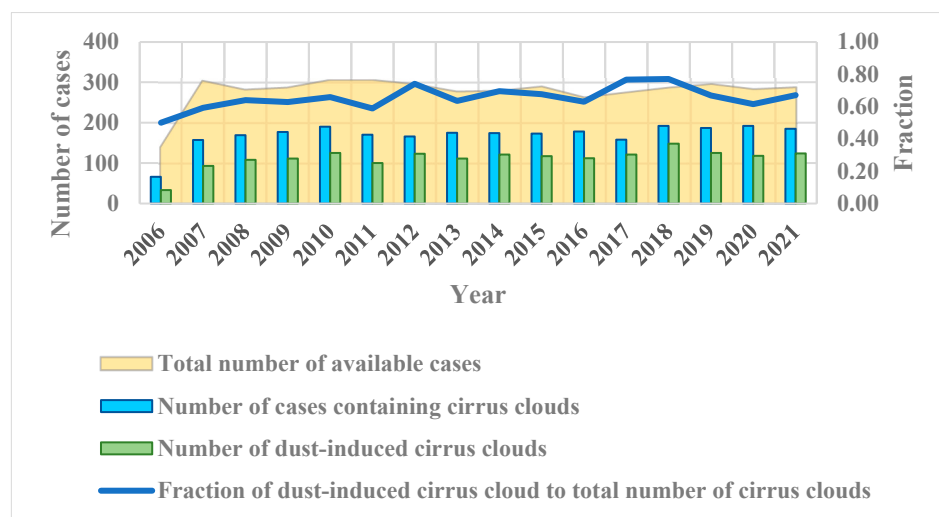


Figure 3. Results for analysis of the Aral Sea in 2006–2021; both day and night data.

To further illustrate, the seasonal average of the different cirrus cloud events for the case study is presented in Figure 4.

To validate the results, the algorithm's outputs are compared with independent observations from the Worldview platform. Results show that 97% of the selected events are verified, which confirms their consistency with the expected conditions for the dust-induced

cirrus cloud formation. The remaining 3% discrepancy suggests areas for further refinement of the detection algorithm, particularly in the cases with outlier conditions. The verification rate of 97% confirms that the algorithm is able to effectively identify high-altitude ice clouds and significant aerosol loading ($AOD > 0.2$) co-exist. This provides a robust and independent confirmation of the atmospheric conditions required for potential dust-induced cirrus formation, thereby substantiating the output of our classification calendar.

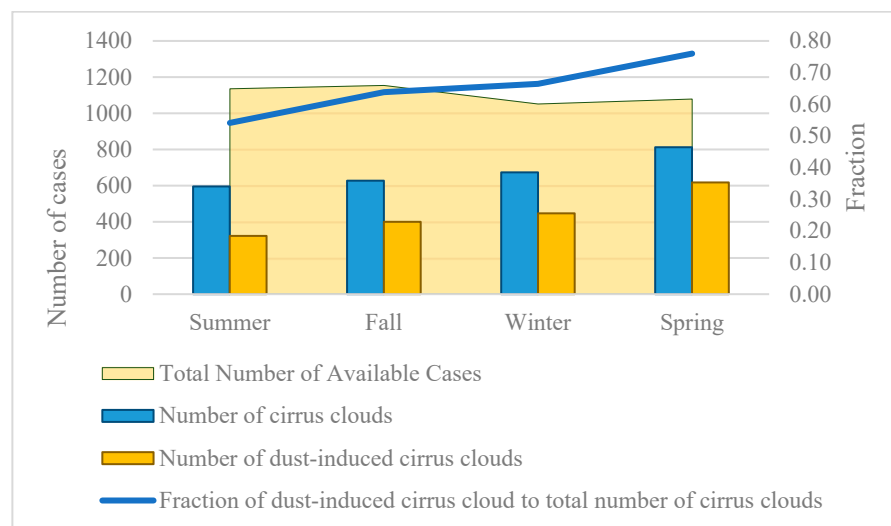


Figure 4. Seasonal average of the events over the Aral Sea region in 2006-2021.

Moreover, analysis of the effect of day and night data on forming dust-induced cirrus clouds is illustrated in Figure 5. Figure 5a shows the total number of cirrus cloud events and dust-induced cirrus clouds from 2006 to 2021 in the Aral Sea region, with a negligible difference. Furthermore, Figure 5b shows the seasonal diagram of the total cirrus cloud events and their proportion by day and night, which is nearly equal in all seasons.

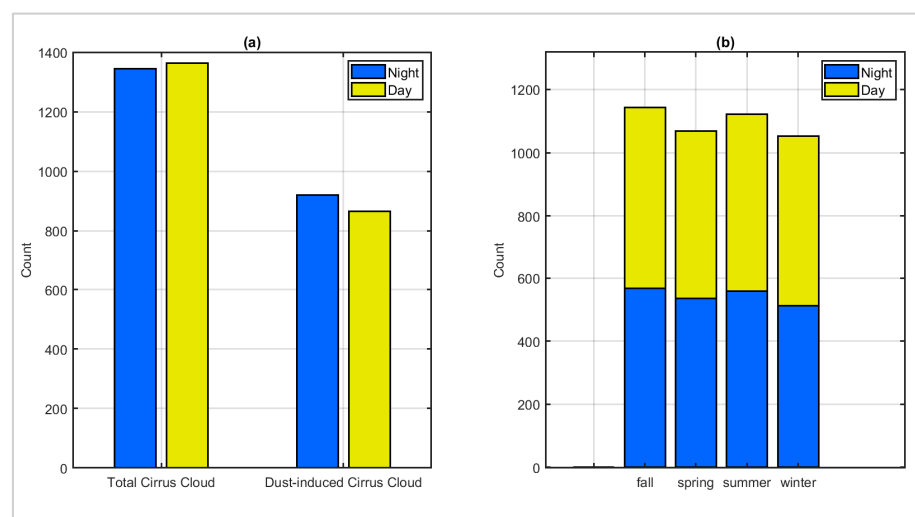


Figure 5. Event occurrences in day and night for (a) total and dust-induced cirrus clouds and (b) seasons for the Aral Sea region from mid-2006 to 2021.

3.2. Iberian Peninsula

For the Iberian Peninsula, 566 cases are identified, with 392 cirrus cloud events that met the required temperature conditions of -33°C and -38°C . Among those, 246 cases (63% of the cirrus events) are determined to be the dust-induced cirrus clouds (see Figure 6). The findings contrast with those from the Aral Sea, underscoring regional differences in

the cirrus cloud formation process. The findings suggest that regional factors, such as proximity to the Sahara and specific atmospheric conditions, play a crucial role in the formation and characteristics of this cloud type.

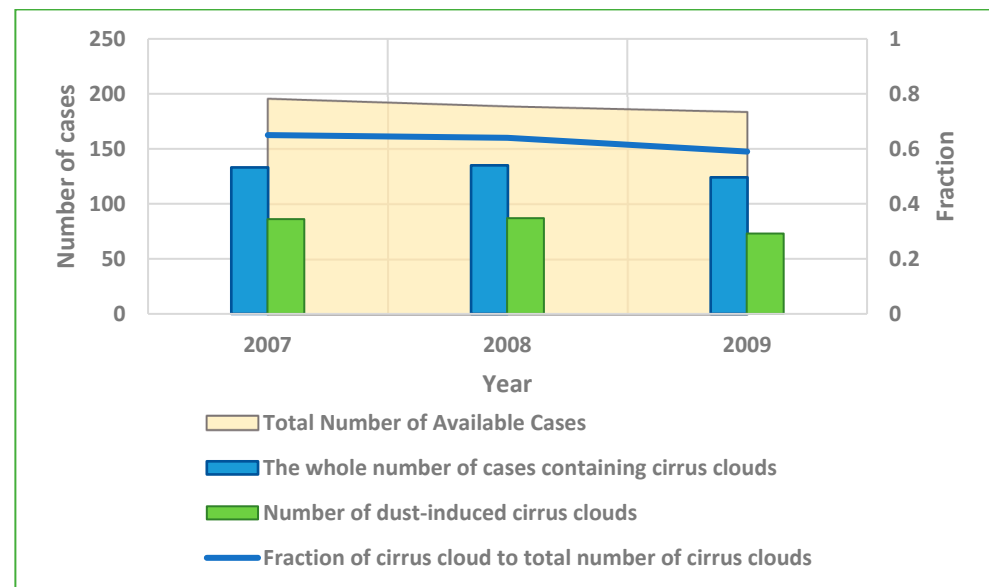


Figure 6. Results for analysis of the Iberian Peninsula case study in 2007–2009; night data.

The Iberian Peninsula case is cross-validated using the Jeggle dataset containing detected cirrus clouds. Table 1 shows that 315 cirrus cloud events are identified as common between the two datasets, providing a reliable foundation for the subsequent analyses. However, a small difference is noted, which could be due to the variations in the temporal resolution of the observations.

Table 1. Cross-validation of the calendar data with the Jeggle dataset for the Iberian Peninsula case.

Year	Number of Cirrus Cloud Events in Calendar	Number of Cirrus Events in the Jeggle Dataset	Number of Events in Common
2007	133	117	114
2008	135	113	109
2009	124	97	92
Summation	392	327	315

3.2.1. Sensitivity Analysis

Given that the algorithm's classification of cirrus clouds is directly dependent on these proximity thresholds, this analysis is essential to confirm that our findings are robust. Results for the threshold change in the detection algorithm for the Iberian Peninsula are presented in Table 2. Results show the events' frequency changes through varying the thresholds in each direction.

Changing the horizontal threshold from 2 km to 4 km in a low-restricted scenario, the algorithm shows a negligible change, with the total number of detected dust-induced cirrus clouds decreasing only by three cases (246 to 243). This indicates that the horizontal dust features interacting with cirrus clouds are overwhelmingly large-scale (>4 km) and that the original findings are not an artifact of a lenient threshold. Conversely, in another scenario, the horizontal requirement to 1 km increased the total count by 58 cases, quantifying a significant population of events associated with smaller-scale dust features.

Table 2. Sensitivity analysis of the dust-induced cirrus detection algorithm for the Iberian Peninsula (2007–2009). The table shows the number of events classified as dust-induced cirrus clouds under different horizontal and vertical threshold scenarios. Changed thresholds in each scenario are shown in bold.

Scenario	Threshold	2007	2008	2009	Total Number of Dust-Induced Cirrus Clouds	Fraction of Dust-Induced Cirrus Clouds to Total Number of Cirrus Cloud Cases (For All Three Years)
Original	2 km horizontal/1 km vertical	86	87	73	246	62.80%
Horizontal change	Low-restricted: 1 km horizontal /1 km vertical	104	107	93	304	77.60%
	Restricted: 4 km horizontal / 1 km vertical	84	87	72	243	62.00%
Vertical change	Low-restricted: 2 km horizontal/ ~0.6 km vertical	95	96	81	272	69.40%
	Restricted: 2 km horizontal/ ~2 km vertical	82	75	65	222	56.60%

The analysis showed moderate sensitivity to the vertical threshold. Making the requirement stricter by demanding a ~2 km deep dust layer reduced the total detections by 24 cases (a ~10% drop relative to the original count). In the low-restricted scenario, the requirement to ~0.6 km increased the count by 26 cases. This indicates that, although vertical depth is an important parameter, the algorithm's output is less sensitive to changes in vertical depth than to variations in the lower bound of the horizontal threshold. Overall, this sensitivity analysis confirms the robustness of our detection method and quantifies the range of uncertainty associated with the threshold. Overall, this sensitivity analysis confirms the robustness of our detection method and quantifies the range of uncertainty associated with the threshold.

3.2.2. Different Properties of Dust-Induced and Normal Cirrus Clouds

Following the categorization of the cirrus events into normal and dust-induced cirrus clouds (described in Section 2.2.1), 208 out of 315 cases (66% of all identified cirrus cloud events) were identified as dust-induced cirrus clouds.

Analysis of the average temperature of the two types of cirrus clouds using MERRA-2 data showed no significant differences between the two cloud categories.

Two cloud types represent distinct properties. As illustrated in Figure 7, dust-induced cirrus clouds, on average, are thicker, form at higher altitudes, and have a greater distance from the cloud top in comparison with normal cirrus clouds. Moreover, dust-induced cirrus clouds are associated with higher values of cloud cover fraction (as presented in Figure 8).

Figure 9 shows the average and variability of three important variables in cirrus clouds. The average mass concentration of the frozen water in the dust-induced cirrus clouds is generally lower than the normal cirrus clouds across all observed years (2007–2009) (Figure 9a,b).

Similarly, the number concentration of the ice crystals larger than 5 μm in the dust-induced cirrus clouds is also lower, except in 2007, which is slightly larger than the normal cirrus clouds (Figure 9b). The effective radius of the ice particles (Figure 9c) is generally the same in the dust-induced cirrus clouds and the normal cirrus clouds. However, in 2008, the average effective radius of the normal cirrus clouds was slightly lower than the dust-induced ones. Additionally, the normal cirrus clouds display a wider range of effective radii, and the total average for the entire time (2007 to 2009) for the dust-induced

cirrus clouds is one unit higher than the normal cirrus clouds. Note that the number concentration of the ice crystals only considers large particles (larger than $5\ \mu\text{m}$). This distinction is crucial because different sizes of the dust aerosols have different effects on the cirrus cloud formation during various growth phases of the cloud [48].

To further illustrate the results, Figure 10 shows a frequency map of the different cirrus cloud events over the Iberian Peninsula during three years (2007 to 2009). Results show that, even in the central parts of the region (e.g., from 4°W to 8°W longitude and from 38°N to 42°N latitude), where dust-induced cirrus cloud events are most frequent, there are still some normal cirrus cloud cases.

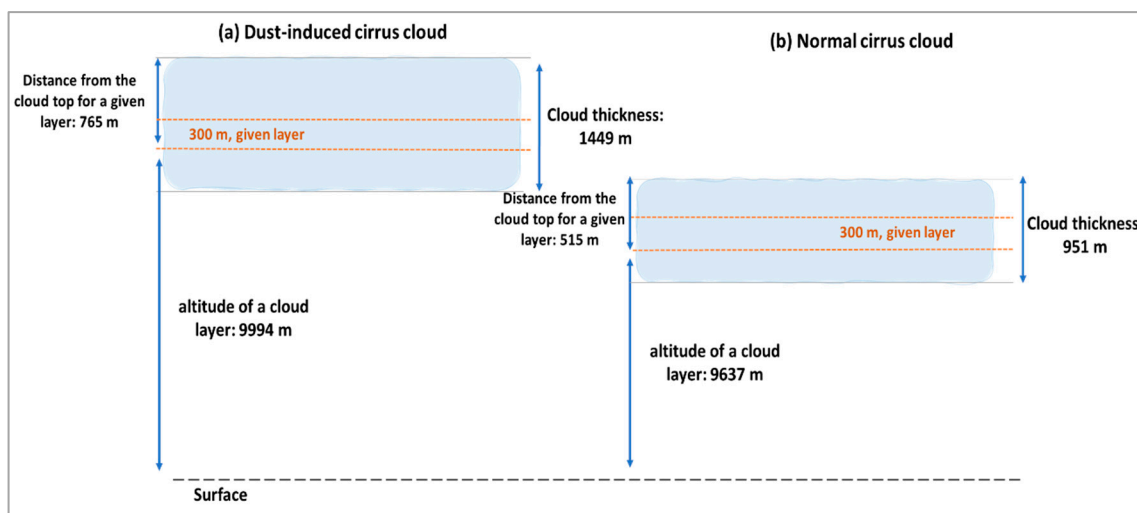


Figure 7. Average values of three variables for two types of cirrus clouds: (a) dust-induced cirrus clouds and (b) normal cirrus clouds. Variables include distance from cloud top for a given layer, cloud thickness, and altitude of a cloud layer from 2007 to 2009; night data over the Iberian Peninsula.

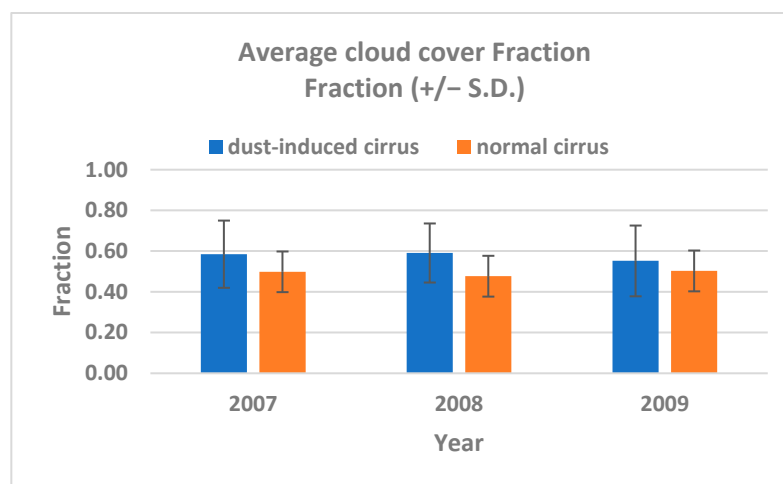


Figure 8. Average values for cloud cover fraction with one standard deviation for the Iberian Peninsula from 2007 to 2009.

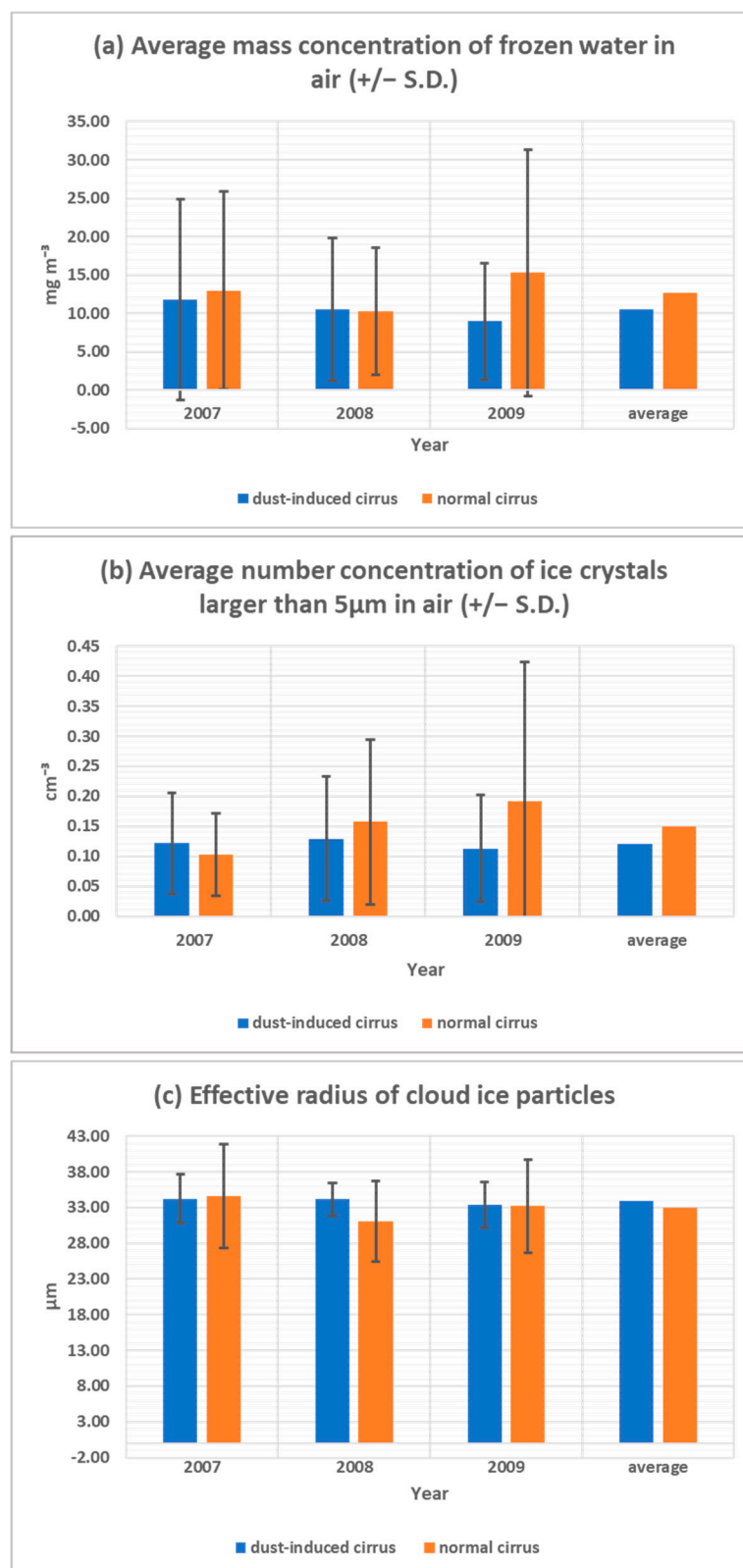


Figure 9. Annual average and box plot distribution for three variables for the Iberian Peninsula from 2007 to 2009. Variables include (a) mass concentration of frozen water in air, (b) number concentration of ice crystals larger than $5\mu\text{m}$ in air, and (c) effective radius of cloud ice particles. Error bars cover ± 1 standard deviation range.

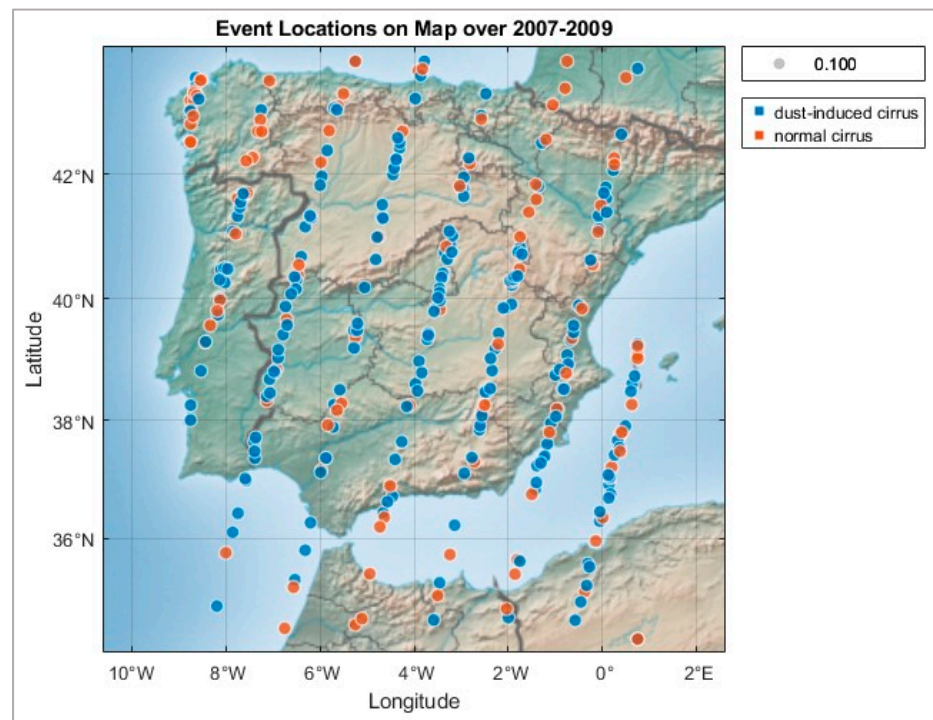


Figure 10. Frequency map of different types of cirrus cloud events in the Iberian Peninsula case from 2007 to 2009.

3.2.3. Statistical Comparison of Cirrus Cloud Properties

To compare the properties of two cloud categories, a statistical analysis is performed on seven key variables for the total 315 common events (with Jeggle dataset; Table 1) in the Iberian Peninsula. The non-parametric Mann–Whitney U test was used to test whether the observed difference between dust-induced and normal cirrus clouds is statistically significant or not. Results of the significance test are summarized in Table 3. It reveals a clear distinction between geometric and microphysical properties. The analysis shows that dust-induced cirrus clouds are associated with geometrically larger properties, with statistically significant differences in cloud thickness, distance from cloud top, altitude of the cloud layer, and cloud cover fraction ($p < 0.001$). In contrast, no statistically significant differences were found for the main microphysical properties. The p -values for ice water content (IWC), ice crystal number concentration (ICNC) larger than $5\ \mu\text{m}$, and effective radius were all above the 0.05 threshold, indicating that the observed variances in these properties are not statistically distinct between the two groups.

Table 3. Statistical analysis of two cirrus cloud categories, dust-induced and normal cirrus clouds, over the Iberian Peninsula in 2007–2009. Statistically significant p -values are shown in bold.

Variable	Cloud Thickness	Distance from Cloud Top	Altitude of Cloud Layer	Cloud Cover Fraction	Ice Water Content (IWC)	Ice Crystal Number Concentration ($>5\ \mu\text{m}$)	Effective Radius
p -value	<0.001	<0.001	0.003	<0.001	0.253	0.66	0.435

4. Discussion

This study develops a systematic classification algorithm on the long-term observational satellite data to provide a statistical basis for understanding how mineral dust influences the frequency of dust-induced cirrus cloud formation. The algorithm examined the properties of the normal and dust-induced cirrus clouds over two key regions. The

analysis reveals a clear distinction between two types of cirrus clouds. Dust-induced cirrus clouds are more frequent than normal cirrus clouds over the two investigated case studies. In addition, results show that, although dust has a statistically significant impact on the geometric scale of cirrus clouds, its effect on the average microphysical state is less direct.

4.1. Prevalence and Regionality of Dust-Induced Cirrus Clouds

Results in Figures 3 and 6 suggest that the cirrus cloud formation in both the Aral Sea and the Iberian Peninsula is closely linked to the presence of the dust particles, leading to the formation of the dust-induced cirrus clouds. The ratio of the dust-induced cirrus clouds to the total cirrus cases (~65%) aligns with the findings of Froyd et al. (2022) [11]. They analyzed cirrus clouds on a global scale and reported varied ratios for different latitudes.

Dust-induced cirrus fractions are subject to variation due to many different variables, such as interannual variability and seasonal differences in temperature, relative humidity, and atmospheric vertical motion [11], which is evident in each year; data are presented in Figures 3 and 6.

The analysis presented in Figure 4 revealed that the dust-induced cirrus clouds are most prevalent during spring, correlating with the highest dust concentrations [33], which is consistent with the study by Froyd et al. (2022) about cirrus formation patterns in the northern hemisphere in different seasons [11]. The seasonal variations and the highest number of cirrus events depend on the location. For example, over Wuhan, China, summer is the most frequent season for the cirrus formation [49]. The results highlight the importance of considering seasonal and regional differences when analyzing the impact of dust on cirrus cloud formation. In this study, the presence of some normal cirrus cloud cases in the central parts of the region, shown in Figure 10, contrary to most frequent dust-induced cirrus clouds in that central area, underscores the effect of other factors, such as temporal variations, that may lead to the formation of the normal cirrus clouds, even within the same geographic location. The findings are consistent with prior studies investigating the role of dust particles in cirrus cloud formation [34,50].

The negligible day–night difference observed in the Aral Sea data (Figure 5) is also explained by the following two factors: first, cirrus cloud formation in the mid-latitudes is often governed by large-scale synoptic systems rather than local diurnal heating [51]; second, combined with the observational constraint of CALIPSO's fixed overpass time (~1:30 a.m./p.m.), which cannot resolve a full 24 h cycle, this fully accounts for our findings [52].

4.2. Different Properties of Two Types of Cirrus Clouds

Categorization of cirrus clouds into dust-induced and normal cirrus clouds allows for a detailed comparison of different properties that could provide insights into the effect of dust particles on cirrus clouds. First of all, we will review the fundamental principles of cirrus nucleation. (1) Homogeneous freezing of supercooled solution droplets, which requires very high supersaturation with respect to ice ($RH_i > 140\%$), typically produces a large number of small ice crystals. (2) Heterogeneous ice nucleation initiated by INPs, like mineral dust, which occurs at a lower RH_i , is expected to produce fewer and larger ice crystals, as their concentration is limited by the availability of INPs. In the following part, the different variables for the two categories are described.

No temperature differences between the two types of cirrus clouds contrast with the studies that reported significant temperature differences in the two cirrus cloud types [18,24]. This contradiction may be due to the fact that the temperature from MERRA-2 in CALIPSO in our analysis overlooks the effect of clouds.

The significant difference between cloud thicknesses (Figure 7) in the two cirrus cloud types confirms findings from other studies that dust-induced cirrus clouds are generally thicker than the normal cirrus clouds [16,24,48]. A study analyzed variations in cloud thickness in case studies with similar dust intensities, in which some cases exhibited dust-induced cirrus clouds and others did not. They hypothesized that the dust-induced cirrus clouds form above the Saharan dust layer through a mixing instability of the air layers. After the initial destabilization at the interface, the longwave cooling induced by the cloud itself drives the turbulent mixing of the layers and the evolution of the shallow convective cirrus [18]. This can explain a higher thickness of the dust-induced cirrus clouds. Furthermore, these clouds seem to form at higher altitudes, as indicated by the average cloud layer altitude, shown in Figure 7, which agrees with the former hypothesis that the dust-induced cirrus clouds form above the Saharan dust layer. In contrast, observational studies suggest that cirrus clouds at lower altitudes are often formed through heterogeneous nucleation, while higher-altitude clouds may exhibit different nucleation characteristics [53]. The findings of this study suggest the presence of competition between two nucleation modes that may influence the cirrus cloud formation across different altitudes. In other words, in cases where both heterogeneous and homogeneous nucleation occur, the competition can result in a wider range of altitudes for cirrus cloud formation [16]. However, the upper parts of these clouds, where homogeneous nucleation might dominate, tend to be at a higher altitude [24,48]. This can also be seen in the cloud thickness, where the dust-induced clouds are thicker, covering more vertical extent.

Higher cloud cover fractions in dust-induced cirrus clouds, as presented in Figure 8, are consistent with the other studies [16]. Efficient ice-nucleating particles can transform significant portions of the supersaturated clear-sky areas into cirrus clouds. These findings have significant implications for climate modeling, as several studies have noted that, without incorporating online dust feedback, their results significantly underestimated the cirrus cloud cover compared with the observations [16,50,51]. Moreover, these four mentioned variables (those in Figures 7 and 8) are a statistically robust finding (i.e., unlikely to have occurred by chance alone) based on Table 3. In contrast to the robust geometric differences, all three variables shown in Figure 9 do not have statistically significant differences between the two cloud categories (Table 3). All of the variables, especially the average mass concentration of the frozen water and number concentration of the ice crystals larger than 5 μm , show high variability. While visual trends in our results are qualitatively consistent with the theory that heterogeneous nucleation produces fewer crystals, the high variability in the data prevents these trends from being statistically distinct when analyzed over a large number of events. This may be attributed to the regional and seasonal variations affecting cirrus cloud properties [11,48], as well as the broad geographic coverage and inclusion of all seasons in the study period. This lack of statistical significance does not negate the role of dust but rather highlights a more nuanced physical reality.

Dust-induced cirrus clouds are typically characterized by lower ice crystal concentrations and smaller particle sizes due to the lower supersaturation levels required for ice formation on the dust particles [5]. The reduced mass concentration of the frozen water in these clouds suggests that the presence of the dust particles might limit the amount of water vapor available for the ice crystal growth, possibly due to the competitive nature of the nucleation process. Conversely, the normal cirrus clouds, which generally form through homogeneous nucleation, require higher supersaturation levels, resulting in a larger number of the smaller ice crystals, which is consistent with the higher ice crystal concentrations and the larger effective radii. Additionally, Seifert, et al. [18] argued for the nonlinear feedback that can reduce the sensitivity of the ice particle number concentration

to the ice-nucleating particles. They mentioned that a high number of ice-nucleating particles may have a minimal impact on the actual characteristics of the clouds, such as the ice particle number, ice water content, or effective radius of the cloud ice particles. Therefore, the differences, high variability, and lack of significant statistical variance in the mentioned variables between the dust-induced and the normal cirrus clouds underscore the complex interactions between nucleation processes.

Homogenous and heterogeneous nucleation, in particular the competition between them, can produce significant variability in cloud microphysical properties, influenced by specific atmospheric conditions such as temperature and humidity [13]. Thus, the precise impact of the dust on cirrus cloud microphysics varies depending on the dominant nucleation processes in each scenario. This issue can be related to the limitation of this study, which is the exclusion of the dust particles below certain thresholds in the vicinity of the cirrus clouds. As mentioned in the methodology (Section 2.2.1), cirrus cloud events are categorized based on the presence of sufficient dust particles near the cloud. However, it is still possible for some dust particles around the cirrus cloud to interact with each other without reaching the level necessary to classify the cloud as dust-induced. Consequently, this hypothesis that all of the normal cirrus cloud events are formed solely by homogeneous nucleation—and that their properties are distinct from those formed by heterogeneous nucleation—is subjected to uncertainty.

4.3. Limitations and Future Work

Despite the robust results, several limitations and uncertainties remain. The reliance on MERRA-2 temperature data, which are not cloud-aware, may affect temperature comparisons. Moreover, variations in dust intensity and meteorological conditions could influence cloud classification. Additionally, the method's dependence on spatial and temporal proximity may not fully capture complex interactions like long-range transport or ice nucleation variations. The primary limitation in classification methodology is the assumption that the spatial co-occurrence of dust and cirrus implies a direct causal link for cloud formation. The algorithm does not distinguish between cases where dust precedes and induces cirrus formation versus instances where a pre-existing cirrus cloud advects into a dust layer. This ambiguity could lead to an overestimation of the frequency of truly dust-induced cirrus clouds. The accuracy of this classification is also dependent on the resolution of the CALIPSO VFM product, and the method's reliance on spatial proximity may not fully capture more complex and non-local interactions. Although our cross-validation confirms the algorithm's ability to detect co-located events, it does not substantiate the causal link for each individual event. Despite cross-validation with independent datasets, differences in data resolution and retrieval algorithms may introduce biases.

Future research should explore the differences between polluted dust and natural dust in the VFM products, particularly their respective impacts on the cirrus cloud properties. Furthermore, expanding the geographical scope of this study and integrating more advanced machine learning techniques could further enhance our understanding of the dust-induced cirrus clouds and their implications for climate modeling. Moreover, considering regional differences for the thresholds, including temperature and the vicinity threshold used in the algorithm, could enhance the study. On the other hand, to more definitively establish causality and validate our classification framework, future work can incorporate air parcel trajectory modeling. Such analysis would allow us to track the history of air masses, confirming whether they pass through known dust source regions before reaching the altitude and location of cirrus formation. Additionally, sensitivity analyses using data from higher-resolution instruments could further enhance the robustness of the findings and provide deeper insights into dust–cirrus interactions over time.

5. Conclusions

This study presents a novel approach for identifying dust-induced cirrus clouds using long-term observational data from CALIPSO and DARDAR-Nice datasets. The proposed algorithm successfully distinguishes between dust-induced and normal cirrus clouds by analyzing the spatial and temporal proximity of dust particles to cirrus clouds. We highlighted the significant role of dust particles in cirrus cloud formation and their distinct properties over two important regions, the Aral Sea and the Iberian Peninsula.

Our findings in the Aral Sea region reveal that a substantial proportion of cirrus clouds are dust-induced, particularly during spring, when the highest dust concentration occurs. This result aligns with previous studies emphasizing the dominant role of the dust in cirrus cloud nucleation. Similarly, in the Iberian Peninsula, a significant fraction of cirrus clouds were found to be dust-induced. Results indicated that these clouds tend to be thicker, form at higher altitudes, and have distinct microphysical properties compared to normal cirrus clouds. Statistical testing using the non-parametric Mann–Whitney U test showed that, while the differences in geometric properties were significant, those for key microphysical properties were not, highlighting a more nuanced physical reality. Findings about differences between these two types of cirrus clouds are in line with the hypothesis that the dust-induced cirrus clouds form above the Saharan dust layer through a mixing instability, where initial destabilization at the interface is followed by longwave cooling from the cloud, driving turbulent mixing and the development of shallow convective cirrus clouds.

This study addressed several limitations in the existing literature. Previous studies have often focused on short-term case studies or specific events, limiting the generalizability of their findings. Using long-term observational data in our study provides a more comprehensive understanding of the dust-induced cirrus clouds across different regions and seasons. Additionally, the use of multiple datasets and cross-validation with independent observations enhances the robustness and validity of our results.

Author Contributions: S.M. (Samaneh Moradikian) performed the data curation and investigation. G.A.H. and S.M. (Sanaz Moghim) administered the project. S.M. (Sanaz Moghim) and G.A.H. obtained the funding and supervised the project. S.M. (Samaneh Moradikian) performed the visualization, wrote the original draft of the manuscript, while S.M. (Sanaz Moghim) and G.A.H. reviewed and edited the manuscript. All authors provided critical feedback and helped shape the research, conceptualization, methodology, analysis, and validation. All authors have read and agreed to the published version of the manuscript.

Funding: This research was funded by the Sharif University of Technology (SUT) through Grant QB020103. This work contributes to and is partly funded by the project PermaStrom within the seventh Energieforschungsprogramm of the German Federal Ministry of Economic Affairs and Climate Action (Bundesministerium für Wirtschaft und Klimaschutz, BMWK) through Grant 03EI4010B.

Data Availability Statement: The collocated data for the Iberian Peninsula were obtained from the dataset by Jeggle et al. (2023), available at <https://doi.org/10.5281/zenodo.7590909>. CALIOP V4.10 data were retrieved from the NASA Langley Research Center Atmospheric Science Data Center at <https://asdc.larc.nasa.gov/project/CALIPSO> (accessed on January 2023). The source code used for the analysis presented in this work will be made publicly available on <https://doi.org/10.5281/zenodo.17102338>.

Acknowledgments: We would like to express our deepest appreciation to Corinna Hoose for her invaluable advice and comments during the project. We acknowledge the use of the CALIPSO dataset, provided by the NASA Langley Research Center's Atmospheric Science Data Center, in partnership with the French Space Agency (CNES). We also acknowledge the DARDAR-Nice dataset, developed through the collaboration between the Laboratoire Atmosphères, Milieux, Observations Spatiales

(LATMOS) and the University of Reading's Department of Meteorology, and made available by the ICARE Data and Services Center. We are also thankful to Jeggle et al. (2023) for providing the open-access dataset. Furthermore, we acknowledge Sharif University of Technology and KIT for their fundings and support.

Conflicts of Interest: The authors declare no conflicts of interest.

References

1. Josset, D.; Pelon, J.; Garnier, A.; Hu, Y.; Vaughan, M.; Zhai, P.; Kuehn, R.; Lucker, P. Cirrus optical depth and lidar ratio retrieval from combined CALIPSO-CloudSat observations using ocean surface echo. *J. Geophys. Res. Atmos.* **2012**, *117*, 5207. [\[CrossRef\]](#)
2. Liou, K.-N. Influence of Cirrus Clouds on Weather and Climate Processes: A Global Perspective. *Mon. Weather. Rev.* **1986**, *114*, 1167–1199. [\[CrossRef\]](#)
3. Yu, P.; Froyd, K.D.; Portmann, R.W.; Toon, O.B.; Freitas, S.R.; Bardeen, C.G.; Brock, C.; Fan, T.; Gao, R.; Katich, J.M.; et al. Efficient In-Cloud Removal of Aerosols by Deep Convection. *Geophys. Res. Lett.* **2019**, *46*, 1061–1069. [\[CrossRef\]](#)
4. Hoose, C.; Möhler, O. Heterogeneous ice nucleation on atmospheric aerosols: A review of results from laboratory experiments. *Atmos. Chem. Phys.* **2012**, *12*, 9817–9854. [\[CrossRef\]](#)
5. Kärcher, B.; Lohmann, U. A parameterization of cirrus cloud formation: Homogeneous freezing of supercooled aerosols. *J. Geophys. Res. Atmos.* **2002**, *107*, AAC 4-1–AAC 4-10. [\[CrossRef\]](#)
6. Jensen, E.J.; Lawson, R.P.; Bergman, J.W.; Pfister, L.; Bui, T.P.; Schmitt, C.G. Physical processes controlling ice concentrations in synoptically forced, midlatitude cirrus. *J. Geophys. Res. Atmos.* **2013**, *118*, 5348–5360. [\[CrossRef\]](#)
7. Hendricks, J.; Kärcher, B.; Lohmann, U.; Hendricks, J.; Kärcher, B.; Lohmann, U. Effects of ice nuclei on cirrus clouds in a global climate model. *JGRD* **2011**, *116*, D18206. [\[CrossRef\]](#)
8. Kärcher, B.; DeMott, P.J.; Jensen, E.J.; Harrington, J.Y. Studies on the Competition Between Homogeneous and Heterogeneous Ice Nucleation in Cirrus Formation. *J. Geophys. Res. Atmos.* **2022**, *127*, e2021JD035805. [\[CrossRef\]](#)
9. Spichtinger, P.; Cziczo, D.J. Impact of heterogeneous ice nuclei on homogeneous freezing events in cirrus clouds. *J. Geophys. Res. Atmos.* **2010**, *115*, 14208. [\[CrossRef\]](#)
10. Kanji, Z.A.; Ladino, L.A.; Wex, H.; Boose, Y.; Burkert-Kohn, M.; Cziczo, D.J.; Krämer, M. Overview of Ice Nucleating Particles. *Meteorol. Monogr.* **2017**, *58*, 1.1–1.33. [\[CrossRef\]](#)
11. Froyd, K.D.; Yu, P.; Schill, G.P.; Brock, C.A.; Kupc, A.; Williamson, C.J.; Jensen, E.J.; Ray, E.; Rosenlof, K.H.; Bian, H.; et al. Dominant role of mineral dust in cirrus cloud formation revealed by global-scale measurements. *Nat. Geosci.* **2022**, *15*, 177–183. [\[CrossRef\]](#)
12. Stocker, T.F.; Qin, D.; Plattner, G.-K.; Tignor, M.M.B.; Allen, S.K.; Boschung, J.; Nauels, A.; Xia, Y.; Bex, Y.; Midgley, P.M. *Climate Change 2013 the Physical Science Basis: Working Group I Contribution to the Fifth Assessment Report of the Intergovernmental Panel on Climate Change*; Cambridge University Press: Cambridge, UK, 2013; pp. 1–1535, ISBN 978-1-107-05799-1.
13. Cziczo, D.J.; Froyd, K.D.; Hoose, C.; Jensen, E.J.; Diao, M.; Zondlo, M.A.; Smith, J.B.; Twohy, C.H.; Murphy, D.M. Clarifying the dominant sources and mechanisms of cirrus cloud formation. *Science* **2013**, *340*, 1320–1324. [\[CrossRef\]](#)
14. Twohy, C.H. Measurements of Saharan Dust in Convective Clouds over the Tropical Eastern Atlantic Ocean. *J. Atmos. Sci.* **2015**, *72*, 75–81. [\[CrossRef\]](#)
15. Voudouri, K.A.; Giannakaki, E.; Komppula, M.; Balis, D. Variability in cirrus cloud properties using a PollyXT Raman lidar over high and tropical latitudes. *Atmos. Chem. Phys.* **2020**, *20*, 4427–4444. [\[CrossRef\]](#)
16. Weger, M.; Heinold, B.; Engler, C.; Schumann, U.; Seifert, A.; Föbög, R.; Voigt, C.; Baars, H.; Blahak, U.; Borrmann, S.; et al. The impact of mineral dust on cloud formation during the Saharan dust event in April 2014 over Europe. *Atmos. Chem. Phys.* **2018**, *18*, 17545–17572. [\[CrossRef\]](#)
17. Hermes, K.; Quinting, J.; Grams, C.M.; Hoose, C.; Hoshyaripour, G.A. Impact of Saharan dust outbreaks on short-range weather forecast errors in Europe. *Q. J. R. Meteorol. Soc.* **2024**, *150*, 1704–1723. [\[CrossRef\]](#)
18. Seifert, A.; Bachmann, V.; Filipitsch, F.; Förstner, J.; Grams, C.; Hoshyaripour, G.A.; Quinting, J.; Rohde, A.; Vogel, H.; Wagner, A.; et al. Aerosol-cloud-radiation interaction during Saharan dust episodes: The dusty cirrus puzzle. *Atmos. Chem. Phys.* **2023**, *23*, 6409–6430. [\[CrossRef\]](#)
19. Huck, R.; Bryant, R.G.; King, J. The (mis)identification of high-latitude dust events using remote sensing methods in the Yukon, Canada: A sub-daily variability analysis. *Atmos. Chem. Phys.* **2023**, *23*, 6299–6318. [\[CrossRef\]](#)
20. Delanoë, J.; Hogan, R.J. Combined CloudSat-CALIPSO-MODIS retrievals of the properties of ice clouds. *J. Geophys. Res. Atmos.* **2010**, *115*, D00H29. [\[CrossRef\]](#)
21. Sourdeval, O.; Gryspeerdt, E.; Krämer, M.; Goren, T.; Delanoë, J.; Afchine, A.; Hemmer, F.; Quaas, J. Ice crystal number concentration estimates from lidar-radar satellite remote sensing—Part 1: Method and evaluation. *Atmos. Chem. Phys.* **2018**, *18*, 14327–14350. [\[CrossRef\]](#)

22. Young, S.A.; Vaughan, M.A. The retrieval of profiles of particulate extinction from cloud-aerosol lidar infrared pathfinder satellite observations (CALIPSO) data: Algorithm description. *J. Atmos. Ocean. Technol.* **2009**, *26*, 1105–1119. [\[CrossRef\]](#)
23. Ansmann, A.; Mamouri, R.-E.; Bühl, J.; Seifert, P.; Engelmann, R.; Hofer, J.; Nisantzi, A.; Atkinson, J.D.; Kanji, Z.A.; Sierau, B.; et al. Ice-nucleating particle versus ice crystal number concentration in altocumulus and cirrus layers embedded in Saharan dust: a closure study. *Atmos. Chem. Phys.* **2019**, *19*, 15087–15115. [\[CrossRef\]](#)
24. He, Y.; Yin, Z.; Liu, F.; Yi, F. Technical note: Identification of two ice-nucleating regimes for dust-related cirrus clouds based on the relationship between number concentrations of ice-nucleating particles and ice crystals. *Atmos. Chem. Phys.* **2022**, *22*, 13067–13085. [\[CrossRef\]](#)
25. He, Y.; Yi, F.; Liu, F.; Yin, Z.; Zhou, J. Ice Nucleation of Cirrus Clouds Related to the Transported Dust Layer Observed by Ground-Based Lidars over Wuhan, China. *Adv. Atmos. Sci.* **2022**, *39*, 2071–2086. [\[CrossRef\]](#)
26. Marinou, E.; Tesche, M.; Nenes, A.; Ansmann, A.; Schrod, J.; Mamali, D.; Tsekeri, A.; Pikridas, M.; Baars, H.; Engelmann, R.; et al. Retrieval of ice-nucleating particle concentrations from lidar observations and comparison with UAV in situ measurements. *Atmos. Chem. Phys.* **2019**, *19*, 11315–11342. [\[CrossRef\]](#)
27. He, Y.; Yi, F.; Yi, Y.; Liu, F.; Zhang, Y. Heterogeneous Nucleation of Midlevel Cloud Layer Influenced by Transported Asian Dust Over Wuhan (30.5°N, 114.4°E), China. *J. Geophys. Res. Atmos.* **2021**, *126*, e2020JD033394. [\[CrossRef\]](#)
28. Jeggle, K.; Neubauer, D.; Camps-Valls, G.; Lohmann, U. Understanding cirrus clouds using explainable machine learning. *Environ. Data Sci.* **2023**, *2*, e19. [\[CrossRef\]](#)
29. Wilks, D.S. *Statistical Methods in the Atmospheric Sciences*; Academic Press: Cambridge, UK, 2020.
30. Hollander, E.C.; Myles, H.; Wolfe, D.A. *Nonparametric Statistical Methods*, 3rd ed.; John Wiley & Sons: Hoboken, NJ, USA, 2014; Volume 11, pp. 1–14.
31. Prospero, J.M.; Ginoux, P.; Torres, O.; Nicholson, S.E.; Gill, T.E. Environmental characterization of global sources of atmospheric soil dust identified with the Nimbus 7 Total Ozone Mapping Spectrometer (TOMS) absorbing aerosol product. *Rev. Geophys.* **2002**, *40*, 2-1–2-31. [\[CrossRef\]](#)
32. Ginoux, P.; Prospero, J.M.; Gill, T.E.; Hsu, N.C.; Zhao, M. Global-scale attribution of anthropogenic and natural dust sources and their emission rates based on MODIS Deep Blue aerosol products. *Rev. Geophys.* **2012**, *50*, 1–36. [\[CrossRef\]](#)
33. Ge, Y.; Wu, N.; Abuduwaili, J.; Kulmatov, R.; Issanova, G.; Saparov, G. Identifying Seasonal and Diurnal Variations and the Most Frequently Impacted Zone of Aerosols in the Aral Sea Region. *Int. J. Environ. Res. Public Health* **2022**, *19*, 14144. [\[CrossRef\]](#)
34. Moradikhan, S.; Moghim, S.; Hoshyaripour, G.A. Development of a dusty cirrus calendar based on satellite data. In Proceedings of the EGU General Assembly 2024, Vienna, Austria, 14–19 April 2024.
35. Córdoba-Jabonero, C.; Lopes, F.J.; Landulfo, E.; Cuevas, E.; Ochoa, H.; Gil-Ojeda, M. Diversity on subtropical and polar cirrus clouds properties as derived from both ground-based lidars and CALIPSO/CALIOP measurements. *Atmos. Res.* **2017**, *183*, 151–165. [\[CrossRef\]](#)
36. Heymsfield, A.J.; Krämer, M.; Luebke, A.; Brown, P.; Cziczo, D.J.; Franklin, C.; Lawson, P.; Lohmann, U.; Mcfarquhar, G.; Mcfarquhar, Z.; et al. Chapter 2 Cirrus Clouds. *Meteorol. Monogr.* **2017**, *58*, 2.1–2.26. [\[CrossRef\]](#)
37. Yorks, J.E.; Hlavka, D.L.; Hart, W.D.; McGill, M.J. Statistics of Cloud Optical Properties from Airborne Lidar Measurements. *J. Atmos. Ocean. Technol.* **2011**, *28*, 869–883. [\[CrossRef\]](#)
38. Holton, J.R.; Curry, J.A.; Pyle, J.A. Encyclopedia of Atmospheric Sciences. *Atmos. Res.* **2003**, *66*, 315–319.
39. Nellore, M.K.; Kannan, V.; Vellaisamy, A.L.R. A statistical method for determining optical and geometrical characteristics of cirrus clouds. *Climate* **2019**, *7*, 72. [\[CrossRef\]](#)
40. Stull, R. *Meteorology for Scientists and Engineers*; The University of British Columbia: Vancouver, BC, Canada, 2005.
41. Zhao, T.X.P.; Ackerman, S.; Guo, W. Dust and smoke detection for multi-channel imagers. *Remote Sens.* **2010**, *2*, 2347–2368. [\[CrossRef\]](#)
42. Li, J.; Ge, X.; He, Q.; Abbas, A. Aerosol optical depth (AOD): Spatial and temporal variations and association with meteorological covariates in Taklimakan desert, China. *PeerJ* **2021**, *9*, e10542. [\[CrossRef\]](#)
43. Payra, S.; Sharma, A.; Mishra, M.K.; Verma, S. Performance evaluation of MODIS and VIIRS satellite AOD products over the Indian subcontinent. *Front. Environ. Sci.* **2023**, *11*, 1158641. [\[CrossRef\]](#)
44. Guerrero-Rascado, J.L.; Ruiz, B.; Alados-Arboledas, L. Multi-spectral Lidar characterization of the vertical structure of Saharan dust aerosol over southern Spain. *Atmos. Environ.* **2008**, *42*, 2668–2681. [\[CrossRef\]](#)
45. Lyamani, H.; Olmo, F.J.; Alados-Arboledas, L. Saharan dust outbreak over southeastern Spain as detected by sun photometer. *Atmos. Environ.* **2005**, *39*, 7276–7284. [\[CrossRef\]](#)
46. Córdoba-Jabonero, C.; Sorribas, M.; Guerrero-Rascado, J.L.; Adame, J.A.; Hernández, Y.; Lyamani, H.; Cachorro, V.; Gil, M.; Alados-Arboledas, L.; Cuevas, E.; et al. Synergetic monitoring of Saharan dust plumes and potential impact on surface: A case study of dust transport from Canary Islands to Iberian Peninsula. *Atmos. Chem. Phys.* **2011**, *11*, 3067–3091. [\[CrossRef\]](#)
47. Maciel, F.V.; Diao, M.; Patnaude, R. Examination of aerosol indirect effects during cirrus cloud evolution. *Atmos. Chem. Phys.* **2023**, *23*, 1103–1129. [\[CrossRef\]](#)

48. Wang, W.; Yi, F.; Liu, F.; Zhang, Y.; Yu, C.; Yin, Z. Characteristics and seasonal variations of cirrus clouds from polarization lidar observations at a 30°N plain site. *Remote Sens.* **2020**, *12*, 3998. [[CrossRef](#)]
49. Krämer, M.; Rolf, C.; Team, C.G.I. A microphysics guide to cirrus—Part 2: Climatologies of clouds and humidity from observations. *Atmos. Chem. Phys.* **2020**, *20*, 12569–12608. [[CrossRef](#)]
50. Diaz, J.P.; González, A.; Expósito, F.J.; Pérez, J.C.; Fernández, J.; García-Díez, M.; Taima, D. WRF multi-physics simulation of clouds in the African region. *Q. J. R. Meteorol. Soc.* **2015**, *141*, 2737–2749. [[CrossRef](#)]
51. Mace, G.G.; Zhang, Q.; Vaughan, M.; Marchand, R.; Stephens, G.; Trepte, C.; Winker, D. A description of hydrometeor layer occurrence statistics derived from the first year of merged Cloudsat and CALIPSO data. *J. Geophys. Res. Atmos.* **2009**, *114*, D00A26. [[CrossRef](#)]
52. Gasparini, B.; Lohmann, U. Why cirrus cloud seeding cannot substantially cool the planet. *J. Geophys. Res.* **2016**, *121*, 4877–4893. [[CrossRef](#)]
53. DeMott, P.J.; Prenni, A.J.; Liu, X.; Kreidenweis, S.M.; Petters, M.D.; Twohy, C.H.; Richardson, M.S.; Eidhammer, T.; Rogers, D.C. Predicting global atmospheric ice nuclei distributions and their impacts on climate. *Proc. Natl. Acad. Sci. USA* **2010**, *107*, 11217–11222. [[CrossRef](#)] [[PubMed](#)]

Disclaimer/Publisher’s Note: The statements, opinions and data contained in all publications are solely those of the individual author(s) and contributor(s) and not of MDPI and/or the editor(s). MDPI and/or the editor(s) disclaim responsibility for any injury to people or property resulting from any ideas, methods, instructions or products referred to in the content.